Fabrication and Characterization of Deformable Porous Matrices with Controlled Pore Characteristics

**Benjamin Munro · Sid Becker · Marc Florian Uth ·
Niklas Preußer · Heinz Herwig**

Abstract The subject of this study concerns a method of manufacture of porous media for which the solid matrix is capable of experiencing deformation under the influence of the flow field. Conventionally, the matrix design parameters, elasticity and pore geometry, cannot be precisely controlled and the choice of parameters is limited to existing available media. Here a solution is provided that uses an indirect solid-free form fabrication process that combines 3D Printing with an infused Polydimethylsiloxane elastomer to provide a highly deformable matrix with controlled pore architecture. The manufacturing method is presented in detail. Local microscopy analysis of the manufactured matrix shows that the method has a high capability to accurately create pore structures at length scales as low as 0.75 mm. Experimental flow measurements further validate that the intended pore geometry is able to be reproduced in highly deformable matrices. The experimentally determined permeability of the deformable matrix is determined to agree with the intended within 95 %.

Keywords Deformable porous media · 3D printing · Manufacture

1 Introduction

In most traditional considerations of flow through porous media, the solid matrix is composed of a very rigid material so that the permeability of the porous media is completely uninfluenced by the flow field. The motivation behind the work of this paper concerns the situation in which the matrix is composed of a material that has a low resistance to deformation. In such a scenario it is reasonable to anticipate that if the pressure gradient associated with the flow field was to be sufficiently large, the pore structure composed by the matrix geometry would respond by deforming. Such deformation would alter the flow path through the matrix,

B. Munro · S. Becker (✉)
Mechanical Engineering Department, University of Canterbury, Christchurch, New Zealand
e-mail: sid.becker@canterbury.ac.nz

M. F. Uth · N. Preußer · H. Herwig
Institute for Thermo-Fluid Dynamics, Hamburg University of Technology, Hamburg, Germany

thereby influencing the ability of the fluid to pass through the porous media. In this paper a rigid matrix that is unlikely to be influenced by the flow field is termed a non-deformable porous media (NDPM). Conversely, a matrix composed of a highly elastic material is called a deformable porous media (DPM).

The applications of flows within deformable porous media occurs across many fields, including drug delivery in living biological media, magma migration, soil consolidation, CO_2 sequestration, and transport processes in human tissue (Ivanchenko et al. 2010; Cowin 1999; Biot and Clingan 1941). It is unsurprising that the theory behind this conjugate fluid-solid interaction has been studied (Cao et al. 2014; Schrefler and Scotta 2001). While much has been realized in modeling the proposed physics of these coupled fluid/solid interactions in deformable porous media, there are very few documented experiments performed in this field that can be used for validation (Schrefler and Scotta 2001; Khan 2010). This is partly due to the challenges that are associated with the fabrication of a deformable matrix. Consider that for a non-deformable (rigid) material, it is easy to fabricate a porous media for which the matrix structural characteristics (pore size, geometry, tortuosity, and porosity) can be specified—for example, by using a 3D printer. To the author's knowledge, however, there is no published robust manufacturing method that allows for a material with a low modulus of elasticity that is highly deformable (elastic) to be used to construct a matrix with specified matrix geometric characteristics.

The existing experimental work in deformable porous media has been limited to use matrices whose local structural characteristics may have a high degree of randomness or variation within the media. The materials used include polyurethane foam (Beavers et al. 1981a, b; Markert 2007), cellulous sponge (Siddique et al. 2009), sand (Biot and Clingan 1941; Biot 1941; Schrefler and Scotta 2001), and aerogels (Boulos et al. 2012; Gross and Scherer 2003). Conventional sponge matrix manufacturing techniques capable of producing these DPM include gas foaming, phase separation, porogen leaching, and solvent casting (Harris et al. 1998; Nazarov et al. 2004; Klempner et al. 2004; Mills 2007; Sauter et al. 2012; Liu and Ma 2009). Using these conventional methods, matrix properties can only be controlled by process and equipment parameters rather than design parameters. For such conventional deformable media, not only are the matrix design parameters (e.g., pore size, geometry, tortuosity, and porosity) non-uniform throughout the media, but also the parameters themselves cannot be precisely controlled or customized.

By contrast to DPM, techniques exist for the manufacture of NDPM that allows for greater control over pore characteristics. The method of solid-free form fabrication (SFF) has received significant attention as a technique that permits the design and fabrication of matrices with controlled architectures (Mikos et al. 2006; Leong et al. 2003; Hutmacher et al. 2004; Hollister 2005). SFF, also commonly known as 3D printing, is a method that involves a layer-by-layer building process from computer aided design (CAD) models (Bourell et al. 1990). There are several different SFF techniques including fiber deposition (Li et al. 2007; Woodfield et al. 2004), selective laser sintering (Williams et al. 2005; Tan et al. 2003; Kruth et al. 2003), stereolithography (Choi et al. 2011; Melchels et al. 2010; Zhang et al. 1999), and fused deposition molding (FDM) (Zein et al. 2002; Kalita et al. 2003). FDM is an extrusion-based process developed by Stratasys, and is among one of the most popular SFF processes. The material in the filament is melted in a specially designed head, which extrudes a layer according to generated section data from a prepared 3D CAD model. As it is extruded, the material cools and solidifies to form a solid. As with other SFF methods, the model is fabricated by stacking and depositing each layer in succession from the bottom to the top.

Porous structures can be created using direct or indirect solid-free form fabrication methods. Direct methods produce the final scaffold directly from the SFF process. During indirect solid-free form fabrication (ISFF) of porous media, the temporary negative molds are fabricated by SFF and used to cast the final matrix (Nguyen et al. 2011). However, these non-random techniques are restrictive in the material that may be used to produce the final matrix, and basically exclude materials for the production of deformable porous media.

Therefore, the aim of this study is to develop a method of manufacturing deformable porous media in such a manner that allows control both over the matrix geometry and the material properties. To achieve this, we consider combining the accuracy and resolution associated with the fabrication of non-deformable porous media in conjunction with a material whose elastic modulus can be controlled. We will show an ISFF method which combines the control and resolution of 3D printing with the deformable material properties of an elastomer. In addition, given that the matrix structure needs to be produced directly from the CAD file, the resolution limits for each step of the manufacturing process are assessed to compare the final matrix with the parameters from the original CAD design using a simple geometry.

2 Matrix Materials and Construction

In this section we describe in detail the indirect solid-free form method of manufacture that we have developed in order to use a material whose modulus of elasticity is variable to fabricate a matrix whose geometrical properties are regular and whose pore geometry can be chosen. We begin with a description of the material chosen for the final matrix and continue with the description of the manufacturing method.

2.1 Matrix Materials

Polydimethylsiloxane (PDMS) is a silicone elastomer with properties that make it well suited for the development of DPM. PDMS is highly elastic while also being linear elastic to strains of 40 %, it is chemically inert, as well being simple to handle and form (Schneider et al. 2009; Mata et al. 2005). PDMS elastomers are attractive candidate's deformable matrix fabrication because their material properties can be altered. Commercially available forms of PDMS (Sylgard 184, RTV 615) typically consist of a two part mixture, a monomer and a hardener. The modulus of elasticity can be altered by varying the mixing ratio of the base polymer to the hardener (Khanafer et al. 2009; Schneider et al. 2008). In the study (Khanafer et al. 2009) the mixing ratio (base to hardener) is varied in order to alter the modulus of elasticity. In that study it is found that a ratio of 6:1 results in an elastic modulus of 0.93 MPa, while a ratio of 9:1 results in a modulus of 1.53 MPa. Another way that the Young's modulus of PDMS can be altered is by varying the curing conditions. For example, in (Johnston et al. 2014) when Sylgard 184 (at a 10:1 mixing ratio) is cured at temperatures 25 °C, the elastic modulus is 1.32 MPa, and when it is cured at 200 °C the modulus is 2.97 MPa. This is of special interest for matrices that are used experimentally as the ability of the matrix to deform can be controlled by specifying the modulus of elasticity. The PDMS chosen for this study was Sylgard 184 (Dow Corning, USA). Two different mixing ratios are employed 10:1 with a measured elastic modulus of 1.58 MPa and a 20:1 ratio with an elastic modulus of 0.35 MPa. The method of evaluating these values of elastic modulus is described in (Khanafer et al. 2009; Schneider et al. 2008).
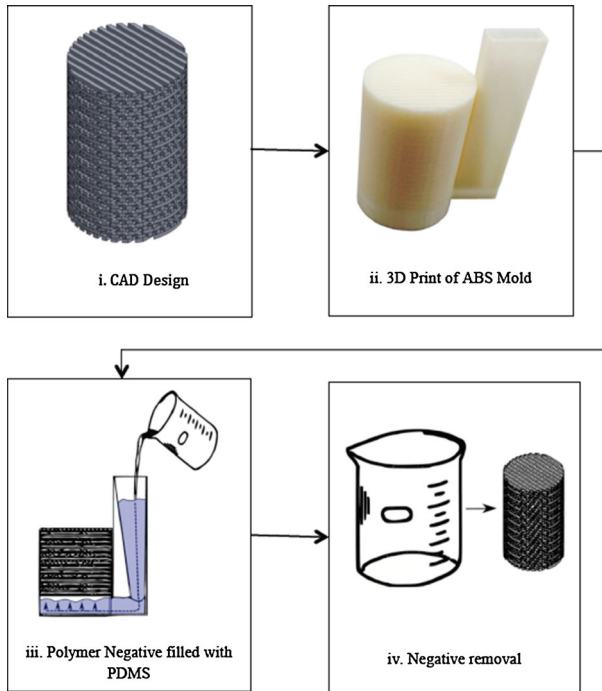
Fig. 1 Illustration of the four step process for manufacture of DPM matrices. *i* Computer aided design (CAD) of a 3D model with the desired matrix architecture; *ii* 3D printing of a negative of the CAD model; *iii* infiltration of the polymer mold with polydimethylsiloxane (PDMS); and lastly *iv* removal of the sacrificial polymer negative

2.2 Manufacturing Method

In order to get the PDMS elastomer into its final form, we developed the following four step ISFF method as illustrated in Fig. 1. These steps involve (i) Computer aided design (CAD) of the 3D model with the desired matrix architecture; (ii) the 3D printing of a hard plastic material from the CAD model; (iii) infiltration and curing of the polymer mold with PDMS; and (iv) removal of the sacrificial polymer negative, by chemical etching. Details of how we used this four step procedure are as follows:

2.2.1 Step (i) CAD

The external scaffold shape and the global porous architecture were designed in the 3D CAD software SolidWorks (Dassault Systemes SolidWorks Corp). The CAD models were converted to stereolithography (STL) files in SolidWorks; CatalystEX (Stratasys Inc.) software then converts the STL file into 3D modeling print paths and generates the support structure with associated print paths. The support structure is used to maintain the shape of the printed object during printing. The exact geometry used in this study is discussed in Sect. 3.1.

2.2.2 Step (ii) 3D Print of ABS Mold

The temporary sacrificial molds were created using 3D printing on a Stratasys Inc. Dimension Elite 3D printer. This will be used later to form the matrix. The mold is non-deformable and
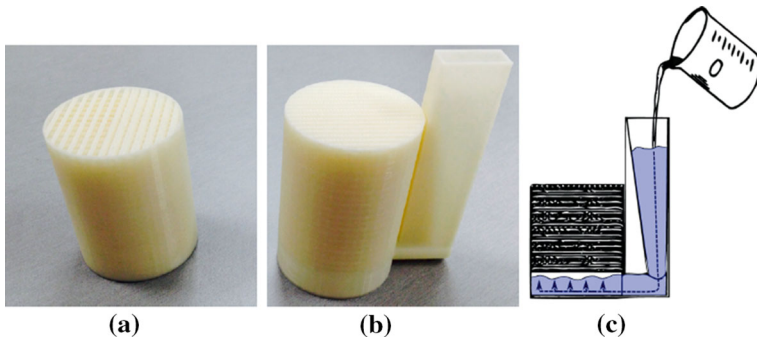
Fig. 2 **a** Original matrix mold where silicon is poured into mold from the *top* **b** Printed ABS matrix mold in which the silicon rises up the mold from the *bottom* **c** Sketch of how the silicon infiltrates the mold under gravity

will reproduce the geometry of the CAD model. The printer extrudes molten acrylonitrile butadiene styrene (ABS) as the build material and SR20 as the support material layer by layer to create the matrix. The matrix should be printed in an ABS plastic without artificial coloring, as this will adversely affect the optical properties of the final deformable porous matrix due to color leaching during removal of the sacrificial ABS mold. The resolution of the printer was set to 0.178 mm and the density to 'solid.' It was found that if lower resolution settings were used, the pores could become obstructed with hairs of ABS. Failure to print the matrix negative at solid density resulted in the struts between the pores becoming porous themselves. After printing, the print support material is to be removed from within the ABS negative so that the mold can be infiltrated. The support structure is water soluble and can be dissolved by submersion in an ultrasonic water bath for nine hours at 70 °C. Once removed from the ultrasonic bath, the ABS mold is washed with ethanol and air-dried.

2.2.3 Step (iii) Infiltration

The PDMS elastomer (Sylgard Elastomer 184, Dow Corning Corporation) consists of a pre-polymer (base) and cross linker. In the results of this study, the silicon elastomer base and the cross linker were mixed at a ratios of 10:1 and 20:1 for five minutes. Air bubbles may appear during the mixing process, thus the mixture is placed in a vacuum chamber (30 kPa (ABS)) for up to 2 h for degassing at room temperature.

When pouring the mixture into the matrix mold, care should be taken to avoid the entrapment of air. The mold is then placed in the vacuum chamber (30 kPa (ABS)) up to 3 h for degassing. To avoid the overflow of PDMS from the mold during degassing, the vacuum was stepped in increments of 10 kPa. Subsequently, the mold is placed into a vacuum oven at 120 °C to cure for one hour. Note that the final material properties of the PDMS elastomer are influenced by the curing conditions (Johnston et al. 2014).

In our earliest attempts, the media was produced by pouring the liquid PDMS into cylindrical molds from the top (see Fig. 2a). The drawback of this method is that air can become trapped in the bottom of the mold under a layer of PDMS. To prevent this, a method was developed by modifying the gravity feed system of Geoghegan et al. (2012) where the PDMS is infiltrated from the bottom of mold. Figure 2b, c shows the new mold.

2.2.4 Step (iv) Negative Removal

After curing is complete, the final step of the process involves removal of the sacrificial 3D-printed ABS negative from the cast PDMS matrix. The ABS is acetone soluble, thus it can be dissolved by prolonged exposure to acetone. Firstly, the cast mold was fully submerged in a 400 ml acetone solution for 8 h to remove the outer layer of ABS. The acetone solution was then replaced and the containing beaker set on a magnetic stirring hot plate for 8 h in order to increase the rate of diffusion of acetone into the matrix. Every 4 h the solution was refreshed as the concentration of the dissolved ABS increases in the acetone solution. The hot plate was set at a constant temperature of 90 °C and the stirrer at a rate of 420 r/min. The matrix is once more left for 12 h in an acetone solution. Finally, the matrix is placed in a sealed container with 100 mL of acetone and gently agitated by shaking every 20 min until all visible ABS plastic has been removed. Replace acetone as needed during this step. The matrix is then left to soak in acetone for 12 h to remove any remaining plastic. Finally, the PDMS matrix was washed with distilled water and dried completely at ambient temperature.

3 Evaluation of the Method

In order to quantify the effectiveness of this method, we have conducted a series of tests that compare the anticipated matrix geometry and behavior to those of the actual PDMS elastomer matrix produced.

3.1 The Matrix Architecture

Here we will describe a very simple matrix design that was tested and implemented. The method described in the previous section allows for a great deal of freedom when specifying the geometric parameters of the matrix, however, to investigate the accuracy of the manufacturing process we have chosen a very simple matrix structure. Four matrices have been produced with identical geometries with different pore sizes, 2, 1.5, 1, and 0.75 mm (Table 1). The matrix architecture used to conduct the following studies was chosen because of its simplicity. The overall concept is that of a matrix that is set in a cylindrical domain (Fig. 3). The structure is based on a repeating base structure (Fig. 3a) that is composed of four variations of a single unit layer (Fig. 3c). The single layer (Fig. 3c) is composed of equispaced parallel square channels in which the width of the pore is equivalent to the width of the solid. The channels are arranged so that they are inversely symmetrical about the channel-wise coordinate passing through the axial center. This means that the spaces filled by a channel on one semi-circular half are represented by the matrix solid on the opposite half resulting in a geometric photo negative. It can be shown that this arrangement allows for a theoretical porosity that is identical to $\epsilon = 0.5$. The base structure is composed of four layers of the unit structure for which the adjacent layers are orthogonal. The channel directions of the bottom two layers are offset from the top by the width of a single pore so that there is no direct path in the global direction of flow (z) across the matrix (see Fig. 3a bottom panel)

3.2 Matrix Characterization at Local Levels

With the purpose of investigating the accuracy of the manufacturing process, the four pore sizes were evaluated to assess the accuracy of the matrix scaffold and pore dimensions. This was achieved by employing scanning electron microscopy (SEM) to sequentially measure
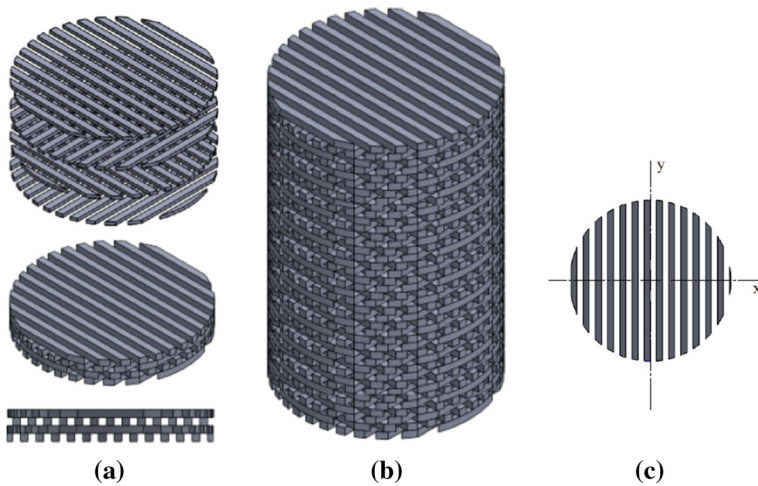
Fig. 3 1.5 mm matrix **a** exploded, isometric and front view **b** full matrix **c** single unit layer

the changes in pore size for each phase of the manufacturing process compared to the original CAD model. The SEM was performed on a Joel JSM-700F SEM. The matrix samples were coated with gold palladium in a vacuum evaporator. Images of the matrix cross sections were taken across the full height of the sample to determine the consistency across the matrix. The average od scaffold and channel size was calculated by processing the images in the image processing package FIJI. This was performed on both the ABS molds and the final PDMS DPM.

Imperfections that are present in the printed mold or that are introduced during the casting of the mold are reflected in the final matrix. Groves orientated perpendicular to the z-axis were present in the ABS mold walls (see Fig. 4a). The grove spacing was 0.178 mm and was transferred to the final PDMS matrix, presenting a corrugated pattern of ridges (see Fig. 4b). These groves are a by-product of the layer-by-layer printing process and as such, have a thickness equal to the printer resolution. Such groves are also evident on the x and y plane, this time due to the extrusion process. The effect of the groves on the flow field is negligible when considering creeping flow.

SEM images have shown that the average pore size of the PDMS matrix is close to that of the predefined CAD model, with dimensional accuracy increasing with pore size. Overall, for the four matrices evaluated, the maximum variation in pore size from the CAD model to the final PDMS matrix was 0.04 mm (5.3 %) (oversize). This was observed in the matrix with the smallest pore size, 0.75 mm. The matrix with the largest pore size, 2 mm, was dimensionally the most accurate.

Because this is a multi-step process, it is necessary to determine which stage of the process contributed to the variation in the final matrix. As can be seen from Table 2, there is a slight reduction in size between the printed ABS mold scaffolds and the CAD model. This difference is 0.01 mm for the 2 mm ABS matrix and 0.02 mm in the other structures. The PDMS infiltration resulted in an increase in pore dimensions for all matrices, and was more pronounced than the decrease in size of the matrix mold during the 3D printing. As for the infiltration phase, the 0.75-mm mold produces the largest percentage change in pore size. The maximum increase was 5.3 % for the 0.75-mm mold. The 2-mm mold produced the smallest variation in dimensions, with an increase of 1.5 % compared to the CAD model.
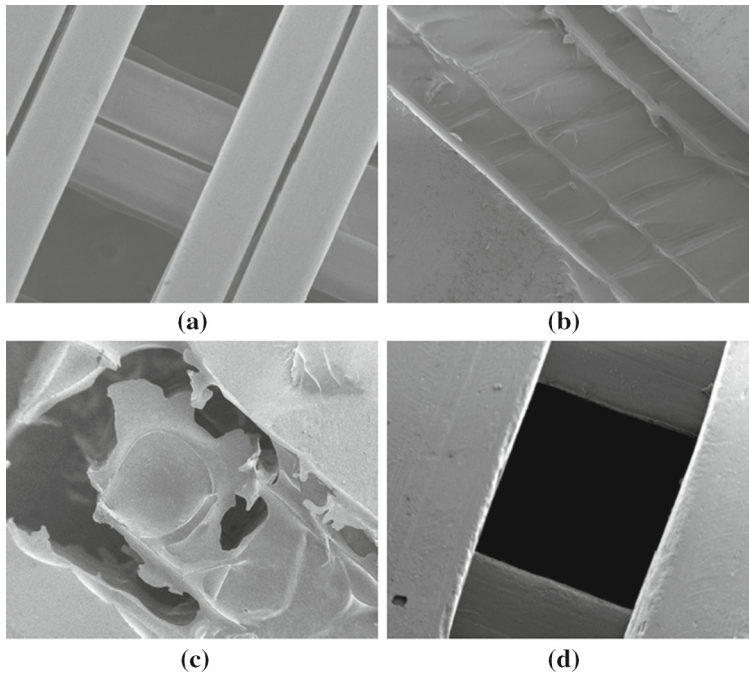
Fig. 4 Matrix imperfections caused during mold printing process: **a** groves in printed ABS mold due to extruded deposition process **b** transfer of mold groves to PDMS matrix causing furrows **c** closed over pores due to PDMS infiltration of low density plastic **d** pore produced under ideal conditions with no printing imperfections

Table 1 Matrix dimension

Pore size (mm)	Wall size (mm)	Overall size (mm × mm)	Porosity
0.75	0.75	45 × 36.9 dia.	0.5
1	1	40 × 36.9 dia.	0.5
1.5	1.5	60 × 36.9 dia.	0.5
2	2	64 × 36.9 dia.	0.5

In general, it was shown by tracking the change in the pore size from CAD model to PDMS matrix, the greatest dimensional errors occurred during the PDMS infiltration phase. The typical increase in channel dimensions was 0.03–0.04 mm for the overall process.

3.3 Porosity Comparisons (Global)

In order to further quantify the effectiveness of this method, we next compare the anticipated porosity to the actual porosity of the matrix. The porosity of the CAD model was determined from the following equation:

$$\epsilon_{\text{theoretical}} = 1 - \frac{V_{\text{solid}}}{V_{\text{total}}}, \tag{1}$$

where V_{solid} (m^3) is the solid volume occupied by the matrix material (excluding the pore volume) and V_{total} (m^3) is the total volume defined as $\pi \cdot \left(\frac{D_{\text{o}}}{2}\right)^2 \cdot \Delta L$, where D_{o} is the outer

Table 2 Channel size comparison between the CAD model, ABS matrix and PDMS matrix

Width of CAD scaffold (mm)	Average width of ABS mold scaffolds (mm)	Difference between ABS and CAD scaffold (%)	Average width of PDMS matrix scaffolds (mm)	Difference between PDMS and CAD scaffold (%)
0.75	0.73 ± 0.01	2.6	0.79 ± 0.01	5.3
1	0.98 ± 0.01	2	1.04 ± 0.01	4
1.5	1.48 ± 0.02	1.3	1.54 ± 0.01	2.7
2	1.99 ± 0.01	0.5	2.03 ± 0.02	1.5

Table 3 Values of porosity for each matrix

D_o (mm)	ΔL (mm)	l_{pore} (mm)	$\epsilon_{theoretical}$	ϵ_{actual}	Variation (%)
39.6	45	0.75	0.5	0.513	2.6
39.6	40	1	0.5	0.514	2.92
39.6	60	1.5	0.5	0.519	3.9
39.6	64	2	0.5	0.520	4.14

diameter of the matrix and L is the overall length of the media. The porosity of the CAD model is 0.5 by definition (see Sect. 3.3). Recall that the choice in matrix geometry of Sect. 3.3 results in matrices of the PDMS and ABS that are theoretically identical, this technical detail allows us to compare to the porosity of the manufactured matrix, directly. To determine the porosity of the fabricated deformable matrix, measurements were taken of length, width, height, and mass of the matrix. The porosity of the matrix was then calculated by

$$\epsilon_{actual} = 1 - \frac{M_{matrix}/V_{total}}{\rho_{PDMS}}, \tag{2}$$

where M_{matrix} (kg) is the measured dry mass of the matrix and ρ_{PDMS} (kg/m^3) is the density of the PDMS (1030 kg/m^3).

Table 3 shows the calculated porosity for the PDMS matrix. The difference in porosity between the CAD model and the PDMS matrix increases as the size of the pores increase. However, there is no significant difference between the porosity of each matrix. The largest difference in porosity occurred in the 2 mm matrix, increasing by 4.14 %. The smallest percentage change on porosity occurred in the 1 mm matrix, with a 2.92 % variation compared to the CAD model.

3.4 Flow Comparisons (Global)

Here we consider that flow through the non-deformable porous matrix and the deformable porous matrix will have identical pressure drops versus flow rate behavior if the following conditions are met:

1. That the DPM in its undeformed state has the same geometry as the NDPM
2. That the flow conditions are such that the pressure drop across the DPM is not sufficient to result in any significant deformation of the matrix

Our intention is to compare the experimentally determined permeability (which is a matrix property) of the flow through the deformable and through the non-deformable porous media

samples. Comparisons between the two values can then be used to provide a means to globally quantify how well our method has reproduced the specified geometry.

The permeability, κ, can be determined experimentally by measuring the pressure drop across the media at a given flow rate and using the constitutive relationships of Darcys law. Darcys law is simply expressed as

$$q = \frac{-\kappa}{\mu} \frac{\partial P}{\partial Z}, \tag{3}$$

where q (m/s) is the average bulk flow rate through the medium, $\frac{\partial P}{\partial Z}$ (Pa/m) is the pressure gradient over the matrix, κ (m^2) is the intrinsic permeability of the porous medium, and μ (Pa·s) is the fluid viscosity. Rearranging for the permeability with the experimentally determined properties gives

$$\kappa = \frac{-u\mu}{\frac{\Delta P}{\Delta L}}, \tag{4}$$

where u (m/s), the flow velocity calculated using the open pipe area and the average volume flow rate, and $\frac{\Delta P}{\Delta L}$ (Pa/m), the measured pressure drop (ΔP) over the matrix length (ΔL), are measured simultaneously for a fluid of known viscosity. Higher Reynolds numbers are avoided in order to remain within the Darcy regime. For this experiment, the Darcy regime is considered to be applicable for flows with a Reynolds number less than 1. The Reynolds number is defined as

$$\text{Re} = \frac{\rho u l}{\mu}, \tag{5}$$

where ρ is the density of the fluid (kg/m^3) and l (m) is the characteristic length. The characteristic length for this definition of the Reynolds number is the ratio between the solid matrix volume and the wetted surface area.

$$l = \frac{V_{\text{pore}}}{A_{\text{wet}}} \tag{6}$$

The wetted area, A_{wet}, is defined as the area of contact between the fluid infiltrating the matrix and the matrix walls and V_{pore} is the total volume encompassing the fluid. For the geometry described in Sect. 3.1, this simplifies to

$$l = \frac{l_{\text{pore}}}{1.5}, \tag{7}$$

where l_{pore} is the pore length (m). It is noteworthy to point out that this expression holds for an infinite medium. However, consider that as noted in Table 3, the outer radial domain is bounded by the diameter $D_{\text{o}} = 39.6$ (mm). As the pore size is increased, the volume to surface area ratio of Eq. (6) will begin to deviate from the value represented by Eq. (7).

A schematic diagram of the experimental apparatus is shown in Fig. 5. The apparatus passes a fluid through a porous media and measures the associated flow rate and pressure drop across the media. An 89:11 glycerol-water mixture was used as the fluid medium. The viscosity of this mixture was 50–60 times higher than the viscosity of water at the same temperature. This allowed us to induce a larger pressure drop across the medium at much lower flow rates, keeping within the Darcy flow regime. Pressure is supplied to the fluid using mains air pressure, which pressurizes the fluid in a pressure vessel. Pressure was controlled manually using a pressure regulator. The pressurized fluid passes through a pipe to the gate valve, which is used to control the flow rate. The fluid is then allowed to pass through the flow meter. Depending on the nominal volume flow rate, the fluid can be diverted through either a fast or slow flow meter before entering a 40-mm Perspex cylinder test section that contains the specimen. The fast flow meter (K400, Piusi) is calibrated to a range of 2–30
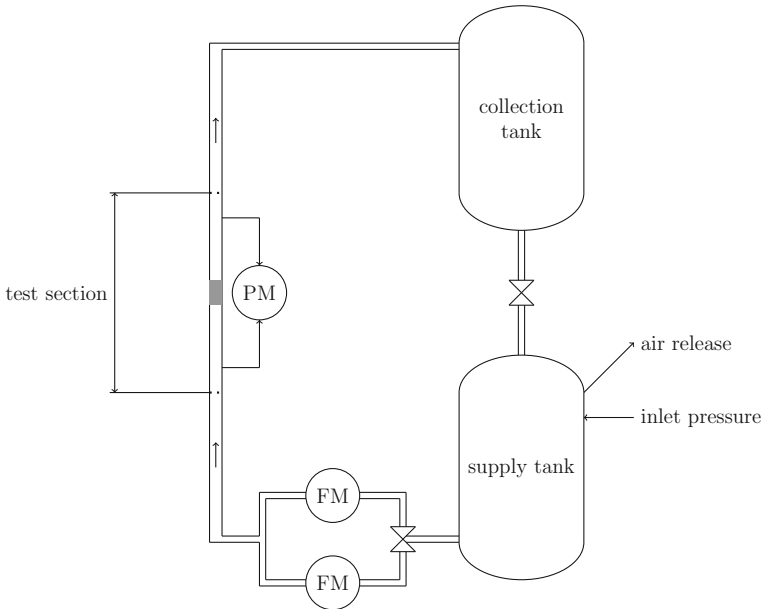
Fig. 5 The experimental apparatus used during this investigation. PM is the differential pressure meter, FM1 is the fast flow meter, FM2 is the slow flow meter and T is the thermometer measuring the glycerol temperature

L/min and the slow flow meter (K200HP, Piusi) is calibrated to a range of 0.10–2.5 L/min. The length of the test section was chosen to allow the fluids velocity profile to reach fully developed conditions before entering the porous medium. The porous media is retained in place by a press fit ring on both the up and down stream faces. Pressure taps were installed into the Perspex cylinder, approximately 50 mm above the upstream matrix face and 60 mm below the downstream matrix face. The pressure taps are connected by hosing to a differential pressure transducer (General Electric, USA) which measures the pressure drop across the pressure taps. The pressure drop due to pipe losses outside the porous media is assumed to be negligible. The pressure transducer has a pressure range of 0–200 bar and maximum pressure differential of 1 bar. Once the fluid has passed the test section it is collected in a reservoir, from which it returned to the supply reservoir post run. Data from the flow meter were collected every 0.1 s, the pressure transducer data were collected every 0.02 s, and data acquisition was managed by a LABVIEW script. The stored data were later processed to obtain the corresponding pressure drop over the media, $\frac{\Delta P}{\Delta L}$, and the average flow velocity, u.

These flow experiments were conducted on matrices with pore sizes of 0.75, 1, 1.5, and 2 mm. The deformable matrices of the 0.75-, 1.5-, and 2-mm pore sizes were prepared with a mixing ratio of 10:1 with a resulting elastic modulus of 1.58 MPa. The deformable matrix of the 1-mm pore size was made with a mixing ratio of 20:1 and a corresponding modulus of elasticity of 0.35 MPa. In Fig. 6, the average fluid velocity is plotted against the measured pressure gradient. Each data point represents the average of at least 1500 measurements of flow rate and pressure drop. The maximum value of the relative standard deviation for any data point from the mean value was 0.79 %. The method of least squares was used to arrive at a linear best fit curve for the data. This is plotted in Fig. 6. Darcy's law was used in the form of Eq. 4 with the slope of the least squares fit to arrive at the permeability of
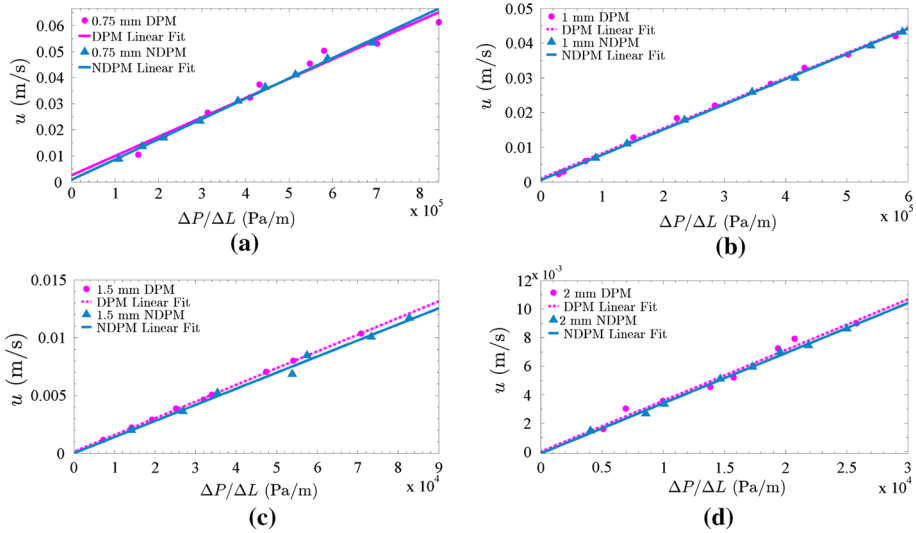
Fig. 6 Plots of pressure drop per unit length against the flow velocity for creeping flows for the 0.75, 1, 1.5 and 2 mm matrices

Table 4 Experimentally determined permeability comparisons

Pore size (mm)	Viscosity (Pa·s)	NDPM permeability (m²)	DPM permeability (m²)	Variation (%)
0.75	0.109	$8.49 \times 10^{-9} \pm 4.5\%$	$8.08 \times 10^{-9} \pm 4.7\%$	4.82
1	0.212	$1.54 \times 10^{-8} \pm 5.1\%$	$1.53 \times 10^{-8} \pm 5.4\%$	0.64
1.5	0.218	$2.95 \times 10^{-8} \pm 6.2\%$	$3.06 \times 10^{-8} \pm 6.3\%$	3.59
2	0.219	$7.69 \times 10^{-8} \pm 4.1\%$	$7.79 \times 10^{-8} \pm 4.2\%$	1.28

each matrix. Table 4 summarizes the permeabilities found for the eight matrices tested. A comparison of the intrinsic permeability between the non-deformable and deformable porous media has shown that the permeabilities are very similar. Because the intrinsic permeability is dependent upon the pore geometry and not the fluid, we can say that the manufactured deformable porous media has a pore architecture close to that defined in the CAD model. Of the matrices evaluated, the maximum difference between the permeabilities if the NDPM and DPM matrices was 4.82 %, which occurred in the 0.75 mm medium. The 1-mm porous medium had the smallest difference, however, there was little disparity between the 0.75, 1, and 2 mm matrices. In Fig. 6a and c there is a distinct offset between the lines of best fit for the non-deformable and the deformable porous media. Overall, the permeabilities of the matrix decrease with decreasing pore size.

4 Application of the Matrix in an Experiment

Recall that the motivation underlying the manufacturing method developed in this paper was to create a deformable porous media for experimental studies. We conclude this paper by showing the ability of a matrix developed using this method to capture deviation from the Darcy regime at very low Re. Keeping the Reynolds number below unity will ensure that
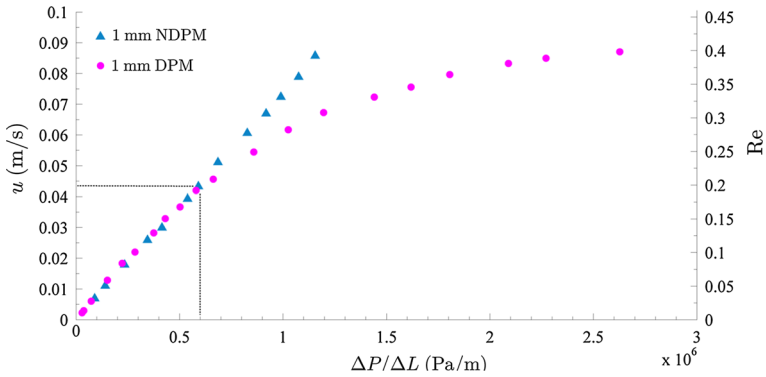
Fig. 7 Comparison of the relationship between DPM and NDPM pressure drop and fluid velocity relationship of the 1 mm matrices. The fluid has a viscosity of 0.217 Pa·s and the DPM elastomer has an elastic modulus of 0.35 MPa. The dashed gray line indicates the limits of data in Fig. 6b

the flow remains well within the Darcy regime and does not transition into the Forscheimer regime. In this way we attempted to ensure that that any experimentally observed non-linearity between pressure and flow velocity is purely due to deformation of the media. Using the experimental test rig described in Sect. 3.4, we present our observations of pressure drop versus flow velocity for $Re < 0.5$. This test was conducted using the 1-mm pore size matrix described in Fig. 3 and Table 3. In this case, a 20:1 mixing ratio was used so that the modulus of elasticity of the elastomer material used to manufacture this matrix is 0.35 Mpa. The results correspond to a matrix whose pore length is 1 mm and the overall matrix length is 40 mm.

Figure 7 shows the comparison between the pressure drop per unit length at a given flow rate for the 1 mm non-deformable media and the deformable media. The deformable media initially shows a linear relationship between pressure drop and fluid velocity. This is anticipated given that the flow is within the Darcy Regime. As the measured pressure drop across the media is increased, however, this linear relationship is no longer seen. At a global Pressure gradient of around 1 MPa/m, the elastic DPM data strongly indicate that Darcy's law is no longer holing: this is indicative of a change in local permeability associated with the deformation of the matrix. At the global pressure gradient of 1 MPa/m the elastomer matrix is exposed to a total pressure drop of 0.04 MPa . This compressive pressure is just over a tenth of the elastomer material's modulus of elasticity, so it is clear that there are sufficient compressive strains to cause deformation of the pore architecture. As the matrix deforms by compression, the pores through which fluid flows are also compressed. This results in a decrease in local permeability which increases the required pressure drop to sustain the flow. As the pressure drop across the elastic DPM is increased, there is less and less of an increase in flow. This is indicative of further compression of the pore geometry.

The results of Fig. 7 present two important points that validate the method of matrix manufacture presented in this paper. Because at low pressure gradients the data comparisons between deformable and non-deformable media tests are very similar, it is likely that the method is able to capture the intended pore geometry in the deformable matrix. The second point is that we were able to create a matrix with this precision using a highly deformable media. That the media is sufficiently deformable is indicated by the non-linear flow behavior at large pressure gradients.

5 Conclusion

In this paper we have presented that our method is able to be successfully implemented in order to manufacture a highly DPM whose pore structure can be controlled with precision. Four matrices were generated with similar geometries but different pore sizes, 0.75, 1, 1.5, and 2 mm that were composed of a highly deformable silicone elastomer. Only minor variations (+0.04 mm) were observed in the channel size compared to the CAD model. Our results show that control of the geometry in the CAD model is reproduced in the final matrix. To further confirm that intended the pore geometry of the deformable media was realized, we experimentally compared the flow behavior of the deformable to the non-deformable porous media samples. The experimentally determined permeability was used as a measure to reflect the pore geometry (an agreement in permeability values would imply similar pore structures). We found strong agreement in the experimentally determined permeabilities for the NDPM and DPM at each pore size. This indicated that the pore geometries were similar and thus close to the architecture defined in the CAD model. Due to the limitations of the ABS mold printing process, this method was limited to pore sizes of 0.75 mm and up; however, strut sizes have been produced down to 0.4 mm indicating room for further improvement. Imperfections that are present in the printed mold or that are introduced during the casting of the mold are reflected in the final matrix. Grooves oriented perpendicular to the z-axis are present in the ABS mold walls. These grooves are a by-product of the layer-by-layer printing process and as such, have a thickness equal to the printer resolution. Post processing of the molds, for example, by brief immersion in acetone, may minimize these imperfections.

References

Beavers, G., Hajji, A., Sparrow, E.: Fluid flow through a class of highly-deformable porous media. Part I: experiments with air. J. Fluids Eng. **103**, 432 (1981a)

Beavers, G., Wittenberg, K., Sparrow, E.: Fluid flow through a class of highly-deformable porous media. Part II: experiments with water. J. Fluids Eng. **103**, 440 (1981b)

Biot, M.A.: Consolidation settlement under a rectangular load distribution. J. Appl. Phys **12**(5), 426–430 (1941)

Biot, M.A., Clingan, F.: Consolidation settlement of a soil with an impervious top surface. J. Appl. Phys. **12**(7), 578–581 (1941)

Boulos, M., Jomaa, W., Sommier, A., Bruneau, D.: An experimental method of characterization of deformable porous media. In: EPJ Web of Conferences, 25, pp. 01006. EDP Sciences, France (2012)

Bourell, D., Beaman, J., Marcus, H., Barlow, J.: Solid freeform fabrication an advanced manufacturing approach. In: Proceedings of the SFF Symposium, pp. 1–7 (1990)

Cao, Y., Chen, S., Meir, A.J.: Steady flow in a deformable porous medium. Math. Methods Appl. Sci. **37**(7), 1029–1041 (2014)

Choi, J.W., Kim, H.C., Wicker, R.: Multi-material stereolithography. J. Mater. Process. Technol. **211**(3), 318–328 (2011)

Cowin, S.C.: Bone poroelasticity. J. Biomech. **32**(3), 217–238 (1999)

Geoghegan, P., Buchmann, N., Spence, C., Moore, S., Jermy, M.: Fabrication of rigid and flexible refractive-index-matched flow phantoms for flow visualisation and optical flow measurements. Exp. Fluids **52**(5), 1331–1347 (2012)

Gross, J., Scherer, G.W.: Dynamic pressurization: novel method for measuring fluid permeability. J. Non-Cryst. Solids **325**(1), 34–47 (2003)

Harris, L.D., Kim, B.S., Mooney, D.J.: Open pore biodegradable matrices formed with gas foaming. J. Biomed. Mater. Res. **42**(3), 396–402 (1998)

Hollister, S.J.: Porous scaffold design for tissue engineering. Nat. Mater. **4**(7), 518–524 (2005)

Hutmacher, D.W., Sittinger, M., Risbud, M.V.: Scaffold-based tissue engineering: rationale for computer-aided design and solid free-form fabrication systems. Trends Biotechnol. **22**(7), 354–362 (2004)

Ivanchenko, O., Sindhwani, N., Linninger, A.: Experimental techniques for studying poroelasticity in brain phantom gels under high flow microinfusion. J. Biomech. Eng. **132**(5), 051008 (2010)

Johnston, I.D., McCluskey, D.K., Tan, C.K.L., Tracey, M.C.: Mechanical characterization of bulk Sylgard 184 for microfluidics and microengineering. J. Micromech. Microeng. **24**(3), 035017 (2014). doi:10.1088/0960-1317/24/3/035017

Kalita, S.J., Bose, S., Hosick, H.L., Bandyopadhyay, A.: Development of controlled porosity polymer-ceramic composite scaffolds via fused deposition modeling. Mater. Sci. Eng. C **23**(5), 611–620 (2003)

Khan, I.: Direct numerical simulation and analysis of saturated deformable porous media. Ph.D. thesis, Georgia Institute of Technology (2010)

Khanafer, K., Duprey, A., Schlicht, M., Berguer, R.: Effects of strain rate, mixing ratio, and stress–strain definition on the mechanical behavior of the polydimethylsiloxane (pdms) material as related to its biological applications. Biomed. Microdevices **11**(2), 503–508 (2009)

Klempner, D., Sendijarevi'c, V., Aseeva, R.M.: Handbook of Polymeric Foams and Foam Technology. Hanser Verlag, Munich (2004)

Kruth, J.P., Wang, X., Laoui, T., Froyen, L.: Lasers and materials in selective laser sintering. Assem. Autom. **23**(4), 357–371 (2003)

Leong, K., Cheah, C., Chua, C.: Solid freeform fabrication of three-dimensional scaffolds for engineering replacement tissues and organs. Biomaterials **24**(13), 2363–2378 (2003)

Li, J.P., Habibovic, P., van den Doel, M., Wilson, C.E., de Wijn, J.R., van Blitterswijk, C.A., de Groot, K.: Bone ingrowth in porous titanium implants produced by 3d fiber deposition. Biomaterials **28**(18), 2810–2820 (2007)

Liu, X., Ma, P.X.: Phase separation, pore structure, and properties of nanofibrous gelatin scaffolds. Biomaterials **30**(25), 4094–4103 (2009)

Markert, B.: A constitutive approach to 3-d nonlinear fluid flow through finite deformable porous continua. Transp. Porous Media **70**(3), 427–450 (2007)

Mata, A., Fleischman, A.J., Roy, S.: Characterization of polydimethylsiloxane (pdms) properties for biomedical micro/nanosystems. Biomed. Microdevices **7**(4), 281–293 (2005)

Melchels, F.P., Feijen, J., Grijpma, D.W.: A review on stereolithography and its applications in biomedical engineering. Biomaterials **31**(24), 6121–6130 (2010)

Mikos, A.G., Herring, S.W., Ochareon, P., Elisseeff, J., Lu, H.H., Kandel, R., Schoen, F.J., Toner, M., Mooney, D., Atala, A., et al.: Engineering complex tissues. Tissue Eng. **12**(12), 3307–3339 (2006)

Mills, N.: Polymer foams handbook: engineering and biomechanics applications and design guide. Butterworth-Heinemann, Oxford (2007)

Nazarov, R., Jin, H.J., Kaplan, D.L.: Porous 3-d scaffolds from regenerated silk fibroin. Biomacromolecules **5**(3), 718–726 (2004)

Nguyen, T.L., Staiger, M.P., Dias, G.J., Woodfield, T.B.: A novel manufacturing route for fabrication of topologically-ordered porous magnesium scaffolds. Adv. Eng. Mater. **13**(9), 872–881 (2011)

Sauter, T., Lützow, K., Schossig, M., Kosmella, H., Weigel, T., Kratz, K., Lendlein, A.: Shape-memory properties of polyetherurethane foams prepared by thermally induced phase separation. Adv. Eng. Mater. **14**(9), 818–824 (2012)

Schneider, F., Draheim, J., Kamberger, R., Wallrabe, U.: Process and material properties of polydimethylsiloxane (pdms) for optical mems. Sens. Actuators A **151**(2), 95–99 (2009)

Schneider, F., Fellner, T., Wilde, J., Wallrabe, U.: Mechanical properties of silicones for mems. J. Micromech. Microeng. **18**(6), 065,008 (2008)

Schrefler, B.A., Scotta, R.: A fully coupled dynamic model for two-phase fluid flow in deformable porous media. Comput. Methods Appl. Mech. Eng. **190**(24), 3223–3246 (2001)

Siddique, J., Anderson, D., Bondarev, A.: Capillary rise of a liquid into a deformable porous material. Phys. Fluids **21**(1), 013106 (2009)

Tan, K., Chua, C., Leong, K., Cheah, C., Cheang, P., Abu Bakar, M., Cha, S.: Scaffold development using selective laser sintering of polyetheretherketone-hydroxyapatite biocomposite blends. Biomaterials **24**(18), 3115–3123 (2003)

Williams, J.M., Adewunmi, A., Schek, R.M., Flanagan, C.L., Krebsbach, P.H., Feinberg, S.E., Hollister, S.J., Das, S.: Bone tissue engineering using polycaprolactone scaffolds fabricated via selective laser sintering. Biomaterials **26**(23), 4817–4827 (2005)

Woodfield, T.B., Malda, J., De Wijn, J., Peters, F., Riesle, J., van Blitterswijk, C.A.: Design of porous scaffolds for cartilage tissue engineering using a three-dimensional fiber-deposition technique. Biomaterials **25**(18), 4149–4161 (2004)

Zein, I., Hutmacher, D.W., Tan, K.C., Teoh, S.H.: Fused deposition modeling of novel scaffold architectures for tissue engineering applications. Biomaterials **23**(4), 1169–1185 (2002)

Zhang, X., Jiang, X., Sun, C.: Micro-stereolithography of polymeric and ceramic microstructures. Sens. Actuators A Phys. **77**(2), 149–156 (1999)